Estimation of the performance limits of a concentrator solar cell coupled with a micro heat sink based on a finite element simulation

Mussad Alzahrani[1,2], Hasan Baig[1*], Katie Shanks[1], Tapas Mallick[1]

[1]Environment and Sustainability Institute, University of Exeter, Penryn Campus, Cornwall TR109FE, UK

[2]Mechanical and Energy Engineering Department, Imam Abdulrahman Bin Faisal University, Dammam, 34212, Saudi Arabia

* Corresponding author: E-mail: h.baig@exeter.ac.uk

Abstract

Concentrated photovoltaic (CPV) technology makes use of cheap optical elements to amplify the irradiance and focus it on small-sized solar cells enabling the extraction of higher amounts of electricity. However, increasing the solar concentration raises the temperature of the PV cell which can deter its performance and can also cause its failure. To combat this issue both active and passive cooling mechanisms are utilized for different types of CPV systems. In this study, we determine the limits of passive cooling systems and establish when an active cooling system is needed based on the recommended operating temperature of the solar cell. We investigate the temperature characteristics of the solar cells bonded to three different substrate materials under different solar concentrations. Results showed that cell temperature is linearly dependent on the concentration ratio and ambient temperature independent of the substrate material. Further, the integration of a micro-finned heatsink results in higher heat dissipation by 25.32%, 23.13%, and 22.24% in comparison with a flat plate heatsink for Direct Bonded Copper (DBC), Insulated Metal Substrate (IMS), and Silicon Wafer (Si wafer) substrates respectively. The low thermal resistance of the IMS substrate compared to the DBC and the Si wafer substrates result in the best thermal performance in terms of maintaining the cell temperature < 80 °C and allowing a wider range of high concentration ratio.

Keywords: Concentrating Photovoltaic, Concentration Ratio, Passive cooling, flat-plate heat-sink, micro fin heat-sink, finite element.

Nomenclature

A	Area (m^2)
Q	Heat dissipated by the solar cell (W)
q	heat flux (W/m^2)
$\dot{q}$	heat source (W/m^2)
q_o	optical power (W/m^2)
T	Temperature (°C)
h	Heat transfer coefficient ($W/ m^2 . K$)
DNI	Direct normal irradiance (W/m^2)
R	Thermal resistance ($m^2.K/W$)
L	thickness (m)
K	thermal conductivity (W/ m . K)
X	The position of fin along the baseplate area (cm)

Greek Symbols

ε	Emissivity
σ	Stefan-Boltzmann constant 5.67×10^{-8} ($W/m^2 . K^4$)
∇	three dimensions (x, y, z)
η	Efficiency

Subscript

s	solar surface
sur	surrounding
a	ambient
c	solar cell
Ge	germanium
Cu	copper
Al	aluminium
Al_2O_3	alumina
Si_3N_4	silicon nitride
SnAgCu	tin-silver-copper
cond	conduction
conv	convective
rad	radiation
tr	Thermal resistance
L	plain layer
baseplate	baseplate area of heatsink
n	number of fins

Abbreviations

DBC	Direct Bonded Copper
IMS	Insulated Metal Substrate
Si Wafer	Silicon Wafer
PCB	Printed Circuit Boards
CPV	Concentrated Photovoltaic
WCC	Worst-Case Condition

1. Introduction

A concentrator photovoltaic (CPV) system replaces expensive, high-efficiency semiconductor materials with cost-efficient optical concentrators[1] with an aim to lower the Levelized Cost of electricity compared to standard solar panels. Single junction silicon solar cells although widely utilized due to their availability and affordability have performance limitations in areas with high DNI and temperature[2] and have been primarily utilized for Low Concentration Photovoltaic Systems. Multijunction solar cells, on the other hand, have better tolerance to extreme DNI and can very well operate at high temperatures and solar concentrations and are essential in any type of High Concentrating Photovoltaic system (HCPV). Currently, multijunction solar cells have been reported to have an efficiency of 47.1% under a solar concentration of 143 suns. These cells optimize the bandgap energy to expand the absorption range of the solar spectrum resulting in less thermalization loss (low thermal performance)[3]. One of the major issues however in the HCPV systems is the dissipation of the excess heat generated due to the limited electrical conversion of the solar energy. Increasing the concentration ratio enables higher power extraction using a smaller solar cell but at the same time increases their operating temperature. The solar cell temperature's linear correlation with the concentration ratio is dependent on the cell area, where increasing the cell area increases the wasted heat [4]. The most commonly used solar cell sizes include 3×3 mm^2, 5.5×5.5 mm^2 and 10×10 mm^2 with peak efficiencies of 42.5%, 41.6% and 40.9% respectively[5]. The performance of a CPV module is strongly influenced by the cell temperature and it is highly desirable to maintain it between 50 – 80 °C [6]. Use of optical concentrators results in localized heated spots due to the nonuniformity of solar irradiance at which mechanical failures such as cell surface deformation might occur[7].

The solar cells are typically mounted on heat spreaders made using highly thermally conductive materials which serve at the same time as contact pads for the internal electrical connection of the module. The thermal behavior of the solar cell mainly depends on the heat spreader type and the associated different layers of the materials employed in its assembly. The heat spreader is located between the PV cell and cooling mechanism to conduct the heat and then dissipate it, as shown in Figure 1

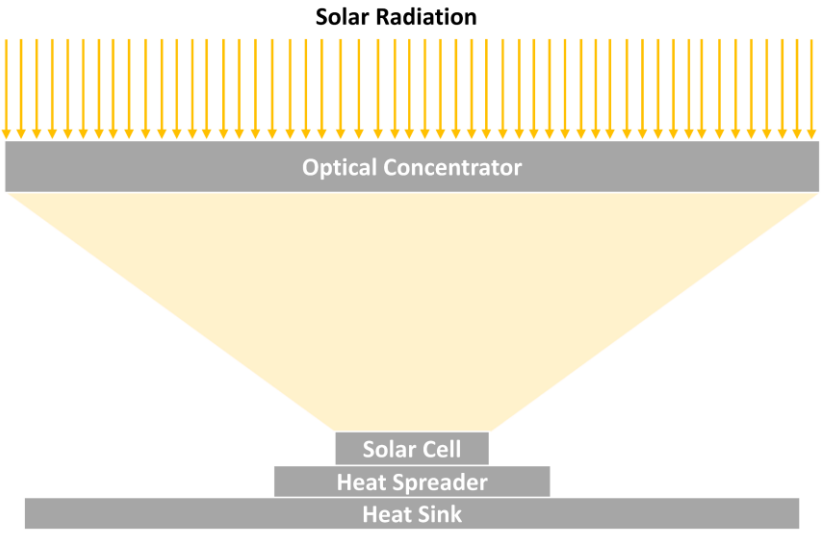

Figure 1 Basic Configuration of a CPV Unit.

The heat sink which is typical of a larger area helps further dissipate the heat to the surroundings. Active and passive cooling mechanisms can be utilized within the heat sink enabling better control of the operating solar cell temperature [8]. Traditionally, passive cooling systems have shown good potential for maintaining temperatures of the PV cell at high concentrations of up to 500 × in severe weather conditions [9,10]. Active cooling, in particular, has been utilized for HCPV systems enabling co-generation of both heat and electricity simultaneously[11–14]. A number of studies have been reported earlier that [15–17] illustrates different cooling mechanisms which have been integrated into CPV systems to maintain the cell temperature below the cell's operational limits. Min et al.[18] developed a thermal model to study a 3 × 3 mm^2 triple-junction solar cell and found the cell temperature reached 1200 °C at 400 suns with no heatsink.

Gualdi et al. [19] identified the limits of passive cooling for concentration ratios up to 2000 suns. Results showed that a flat heat-sink could maintain the cell temperature below 80 °C for a cell side length between 2-4 mm. A thermal test and simulation of an Alumina flat heat-sink for a concentration ratio in the range from 1 sun up to 1000 suns showed that at 500 suns the cell temperature reached 80 °C and kept increasing to reach about 120 °C at 750 suns[20]. Wang et al.[21] presented a numerical investigation addressing the effect of DNI, the wind speed, the module elevation angle, and the ambient temperature. Renzi et al. [22] studied the performance of two commercial 3.5 kWp CPV systems at 476 suns. The temperature of the backside of the aluminum heatsink was measured to be in the range of 55 and 65 ℃. Chou et al.[23] developed a thermal model to assess the performance of a 6.5 × 5.5 mm^2 triple-junction solar cell under a concentration ratio of 380 suns cooled with an aluminum flat-plate heatsink

and reported the maximum cell temperature of 69℃ correspondent to the thermal resistance of 4.67°C/W. Theristis and Donovan [24] used finite element analysis to estimate the operating temperature of a 10 × 10 mm^2 triple-junction solar cell and found that the flat plate heatsink of 1.63 K/W thermal resistance can passively maintain the solar cell in a safe operating condition up to 500 suns. A further study showed that a solar cell of 1 × 1 mm^2 or below with an aluminum flat-heatsink could maintain the cell temperature below 60 °C [4]. Micheli et al. [25] showed that the optimized fin array improved the mass-specific power by up to 50%. Further, they explored the use of different substrate materials like DBC and, IMS [5].

Abo-Zahhad et al. [26] developed a thermal model to investigate effect of increasing the area ratio (proposed two copper areas/originally defined two copper areas). Hu et al.[27] studied the dynamic performance of a hybrid system coupled subsystems The subsystems helped to maintain the electrical efficiency to 35.15% with a tank water mass altering range between 0.82-17.52L. Abo-Zahhed et al. [28] examined novel jet impingement microchannel heatsink design and compared it with a conventional model.. Maka and Donovan [29] reported that, at 1000 concentration ratio, a minimum of 2400 W/m^2. K of the convective heat transfer coefficient is needed to maintain the cell < 80 °C.

Aldossary et al. [30] studied two passive cooling designs (round pin and straight fins heatsinks) and showed that they are incapable of maintaining the cell temperature < 80 ℃. Wang et al. [31] reported that the temperature could be maintained below 75℃ at the worst ambient temperature of 45℃ with a fan pump power of less than 2W.

Fin heat-sinks are widely used to enhance the heat transfer between two media by the thermal exchanging surface. Parametric optimization for fin heat-sink geometry in CPV application showed that a thicker fin does not improve the heat transfer because of the surpassing convective heat transfer between fins[32,33]. A thinner fin in a heat-sink with an optimized fin number minimizes the weight. The minimized weight of the heat-sink materials reduces the load and size of the tracking system, especially with a high and ultra-high concentration ratio, where the acceptance angle is limited. The optimization of the fin number and fin spacing is strongly related to the temperature difference and inclination angle[34–36]. In a micro fin heat sink, a general correlation among geometry and orientation has been experimentally studied and showed that convective heat transfer coefficient increases by decreasing the height of the fins, increasing the fin spacing, and/or decreasing the fin thickness for upward/ downward horizontal orientation and vertical orientation, as in Figure 2. The

upward horizontal orientation showed a 12% discrepancy in the thermal resistance compared to the downward surface orientation. Kim and Micheli [37][38] carried out their experimental study at 100 – 200 micrometer-height and their work showed an enhancement in the thermal exchange of up to 10%. Also, the correlation between the fin's geometry and thermal performance was investigated for a range of temperatures [39,40]. Recently, flared heatsink configurations applied in CPV module were experimentally investigated and showed a reduction in the thermal resistance of 10 % in comparison to a flat-plate heat sink [41].

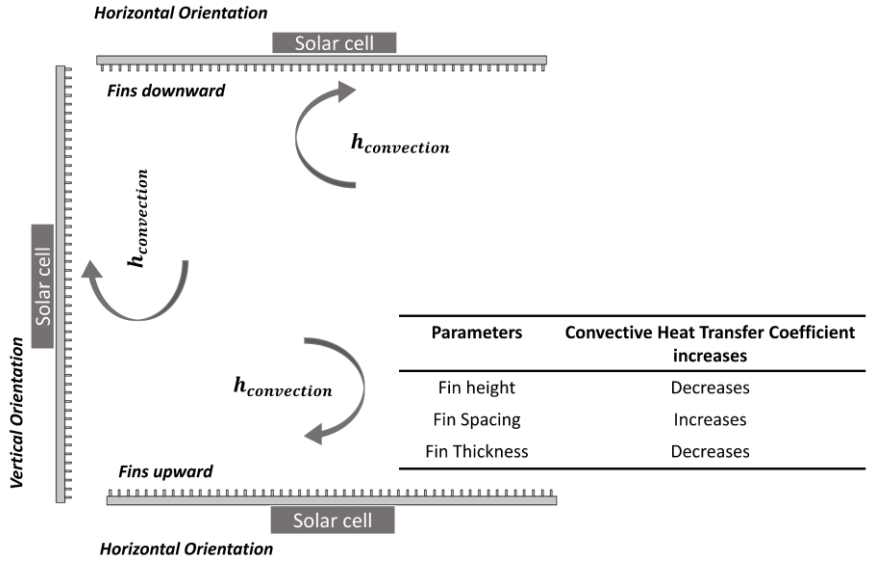

Figure 2 General correlation between geometry and orientation for micro-fin heat-sink [34–36].

In this study we report the influence of different parameters that dictate the solar cell operating temperature. The concentration ratio in the range of 100 -1000 suns has been investigated for the worst-case operating condition on a 3 × 3 mm^2 multijunction solar cell bonded to a flat-plate and micro fin heat-sink. The use of three different substrate materials namely Direct Bonded Copper (DBC), Insulated Metal Substrate (IMS), and Silicon Wafer substrate (Si wafer) has been explored. For the micro-fin heat-sink, the effect of wind speed on the external boundaries has been taken into consideration by varying the convective heat transfer coefficient between $3 - 25\ \left[\frac{W}{m^2.K}\right]$ [42]. The impacts of extreme weather conditions have been considered by varying the ambient temperature beyond 50°C. Furthermore, a geometrical parametric study for heat sink fin number and fin spacing has been numerically investigated to optimize the thermal performance. The results help determine the concentration ratio limits at which passive cooling is no longer enough and active cooling is needed to thermally manage the solar cell for improved reliability.

2. CPV design considerations

A starting point for the design of any CPV system is to determine the type of solar cell used and its associated heat dissipation system. A clear understanding of the expected environmental conditions can help determine the solar cell operating temperatures, the amount of power to be extracted and the overall physical dimensions of the system depending on the type of heat sink deployed. The cell temperature's linear correlation with the concentration ratio is dependent on the cell area, where increasing the cell area increases the wasted heat.

In this study, a 3×3 mm^2 multijunction PV (Model 3C44C) cell from Azur space has been considered as shown in Figure 3. The cell is designed to operate within a range of 100-1500 suns and has a peak efficiency of 42%. The maximum operating temperature is reported to be 110 °C [43]. The cell has a widely recognized H-pattern optimized to perform under non-uniform illumination conditions.

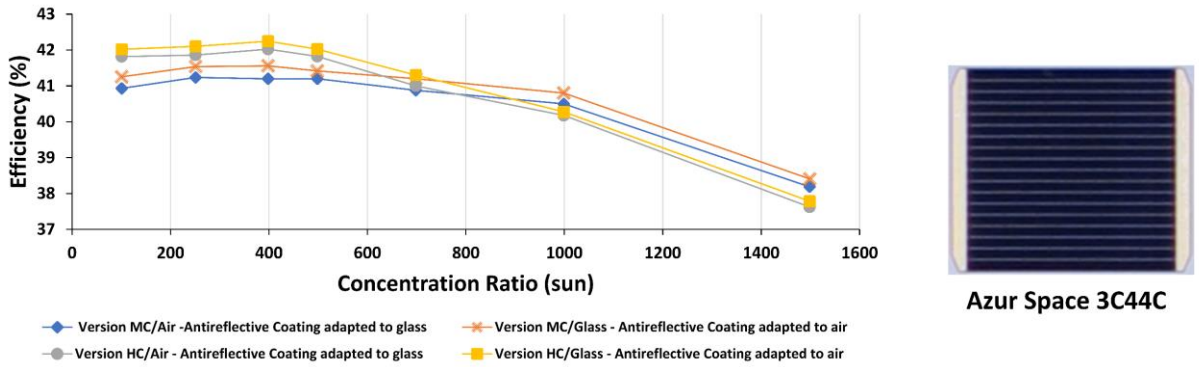

Figure 3 Performance characteristics of an Azur space 3C44C. The four lines are efficiency versus sun concentrations for version MC/air & glass and version HC/Air & glass where the solar cell is optimized. Measurement conditions is 1.5 AM D – 1000 W/m2 (ASTM G 173-03), T = 25 °C, designated measurement area = 100,51 mm² [43].

2.1 Passive cooling with fin design

Utilization of passive cooling mechanisms in different studies has been proven to successfully handle the thermal management for a wide range of concentration ratio. Flat-plates and finned heat-sinks are used commonly in a passive cooling system. Generally, increasing the area of the heat-sink baseplate easily dissipates heat but at the cost of increased module weight which ultimately increases the cost of tracking and the LCOE ultimately. So, the minimum heat-sink

baseplate area for Azur Space 3C44 – 3 × 3 mm^2 cell area is calculated, applying the same approaches in [5], by the Eq.(1).

$$A_{baseplate} = \frac{Q_C}{[q_{conv} + q_{rad}]} \quad (1)$$

The CPV system exchanges heat with its surrounding through natural convection and radiation. The convective heat flux (q_{conv}) is proportional to the difference between the solar surface temperature (T_S) and the ambient fluid temperature (T_a) considering the exchange baseplate area ($A_{baseplate}$) and the convective heat transfer coefficient (h), as in Eq.(2).

$$q_{conv} = A_{baseplate} . h . (T_s - T_a) \quad (2)$$

Where radiation (q_{rad}) is proportional to the difference between the solar surface temperature (T_S) and the surrounding fluid temperature (T_{Sur}) to the fourth power considering the radiative property (ε) of the exchange baseplate area ($Area_{baseplate}$) and the Stefan-Boltzmann constant ($\sigma = 5.67 \times 10^{-8} \frac{W}{m^2.K^4}$), as in Eq.(3)

$$q_{rad} = A_{baseplate} . \varepsilon . \sigma \left(T_s^4 - T_{Sur}^4\right) \quad (3)$$

Assuming that all the heat generated (Q_C) by Azur Space 3C44C – 3 × 3 mm^2 cell is conducted to the bottom surface of the heat sink, considering only the flat bottom surface of the receiver, and taking into account the highest value of natural convective heat transfer coefficient of 25 $W/m^2.K$, an emissivity value of polished aluminum surface of 0.09, a heat sink surface temperature of 60 ℃, and an ambient temperature of 25 ℃. Thus, the minimum required dissipating area of 0.0025 m^2 is required correspondent to 5 × 5 cm^2. The assumption was made considering the emissivity value of aluminum instead of copper and silicon where they would result in the lesser dissipating area due to their higher emissivity. The fin heat-sink geometry is obtained from[25], as in Figure 4. A 3x3 mm^2 multijunction solar cell is attached to a heat sink with an area of 25cm^2 and uses 50 micro-fins (thickness 200μm and pitch of 900μm).

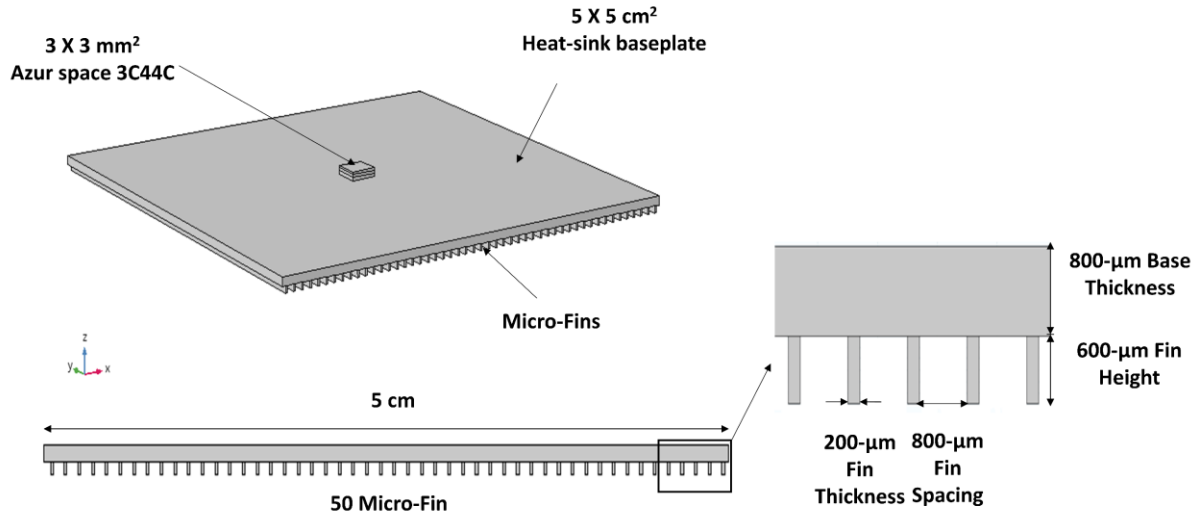

Figure 4 Asymmetric, side-view, and cross-section view for the micro-finned heat-sink with typical dimensions of the fins

2.2 Heat Spreader selection and thermo-physics Properties

The selection of the CPV system's components and materials plays a fundamental role in thermal management. The heat spreader between the PV cell and the heat-sink needs to be highly efficient to transfer the generated heat out of the PV cell. A high thermal conductivity material for the substrate is preferable, while electrical conductivity needs to be minimized. The most commonly used substrate in the CPV system is Direct Bonded Copper (DBC) due to its mechanical strength and excellent thermal and electrical properties[44–46]. Printed Circuit Boards (PCB) substrates on the other hand which is widely used in the electronic applications have a laminated fiberglass on one or both sides with copper that decreases the thermal conductivity[47] and limits its application in CPV. Replacing the laminated material with a metal improves the thermal conductivity and is referred to as Insulated Metal Substrate (IMS). IMS is an alternative for DBC due to its affordability and excellent thermal performance[48]. Also, Silicon wafer (Si wafer) is an excellent material for the substrate because Si wafer has a similar thermal expansion rate to the multijunction PV cell semiconductor material that can improve its reliability [5]. Silicon manufacturability is simple, but silicon is an expensive material compared to other substrates and mechanically fragile[38].

The substrate layer thickness and materials have been selected according to the cell area, as shown in Figure 5.

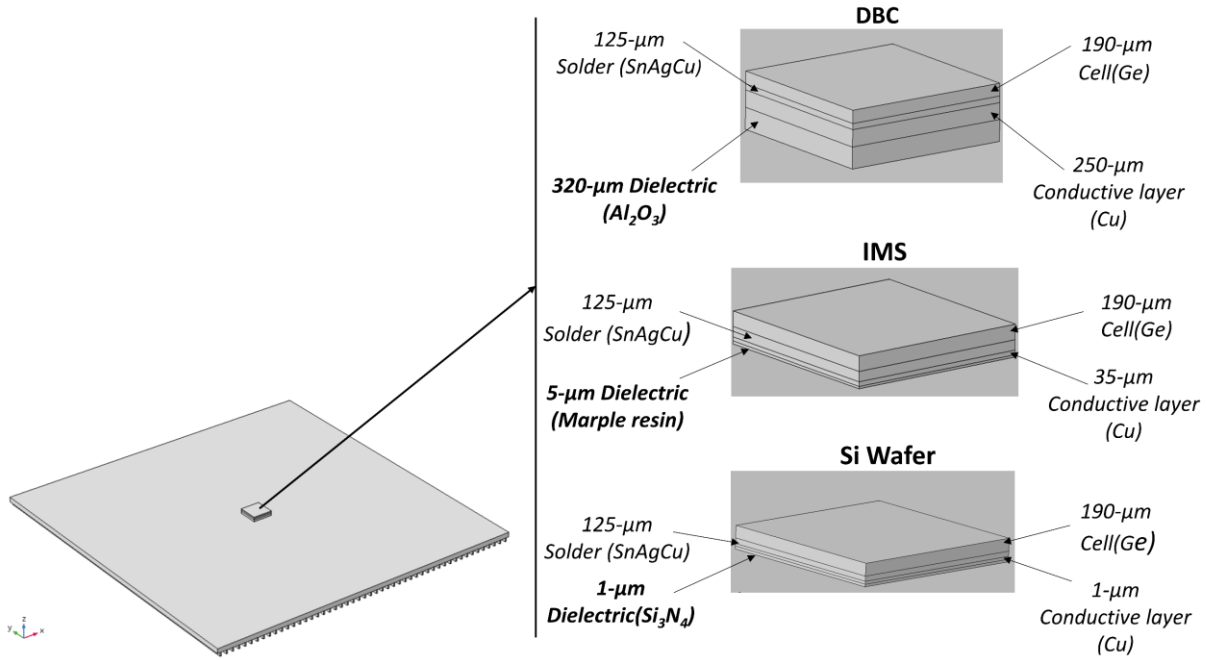

Figure 5 Geometric model of the CPV receivers, material and thickness layers for the DBC [35], IMS [33], and Si wafer [36].

Three different substrates with three different heat-sink materials have been researched in COMSOL Multiphysics to evaluate the thermal performance at fixed heat-sink geometry, as in table 1.

Table 1 Thermo-physical properties used in COMSOL

Material	Density [kg/m^3]	Heat Capacity [J/kg. K]	Thermal Conductivity [W/m. K]
Germanium (Ge)	5323	700	60
Copper (Cu)	8700	385	400
Aluminium (Al)	2700	900	238
Silicon (Si)	2329	700	130
Alumina (Al_2O_3)	3900	900	27
Silicon nitride (Si_3N_4)	2370	673	10
Marble Resin	-	-	3

3. Numerical Model

In the present study, we model the solar cell and the associated heat dissipation using the energy equation. The heat transfer rate in the CPV unit is governed by considering the energy conservation law for the steady-state condition with the heat source ($\dot{q}$), where (q_{cond}) and (q_{conv}) indicate the conduction heat transfer and the convective heat flux, respectively, in Eq. (4).

$$q_{cond} = \dot{q} + q_{conv} \quad (4)$$

The analysis of the conduction heat transfer rate (q_{cond}) in the solid domain is obtained by Fourier's law. The conduction heat transfer equation is solved to obtain the temperature distribution between the solid layers in three dimensions (x, y, z) where it is presented as a del operator (∇) considering the solid layers thermal resistance ($R_{tr,cond}$) in Eq. (5)

$$q_{cond} = \nabla\left(-\frac{1}{R_{tr,cond}}\nabla T\right) \quad (5)$$

The thermal resistance, by different layer composition, influences the heat transfer rate because thermal resistance and thermal conductivity are inversely correlated as in Eq. (6)

$$R_{tr,cond} = \frac{L_L}{k_L} \quad (6)$$

The thermal resistance is basically the reciprocal of the thermal conductivity (K_L) through a plain layer of a thickness (L_L)

The convective heat flux (q_{conv})on the external boundaries is obtained by Newton's law of cooling considering $R_{tr,conv}$ using Eq. (7). However, the adiabatic condition has been applied for the baseplate periphery of the heat-sink taking into consideration the real condition where the receiver is contiguous with other receivers.

$$q_{conv} = \nabla\left(\frac{1}{R_{tr,conv}} . \nabla T\right) \quad (7)$$

The thermal resistance is also associated with convective heat transfer where it is the reciprocate of the convective heat transfer coefficient (hc) in Eq. (8).

$$R_{tr,conv} = \frac{1}{h} \quad (8)$$

The CPV system was mounted in a horizontal position, where buoyancy force is normal to the layer, to allow the natural convection flow and to avoid the temperature gradient on the layer.

Considering the energy conservation law with a heat source for a steady-state condition in Eq. (4), the conduction heat transfer equation for estimating the temperature distribution in the solids can be solved by Eq. (9)

$$\nabla\left(\frac{1}{R_{tr,cond}}\nabla T\right) = \dot{q} \quad (9)$$

The heat source can be modelled as shown in equation (10) below. Where (q_o) indicates the optical power output in (W/m^2) after solar concentration and $(\eta_{electrical})$ indicates the electrical efficiency of the solar cell.

$$\dot{q} = q_o \,.(1 - \eta_{electrical}) \quad (10)$$

The arrangement of the solar cell as a heat source is to model the portion of solar irradiance that converts to wasted heat. The optical power after concentration can simply be expressed as the product of the direct normal irradiance available, the geometric concentration factor and the optical efficiency. For a worst-case condition, we consider that the solar cell generates no electrical energy and assume that all the available optical power is to be dissipated by the heat sink. The optical efficiency $(\eta_{optical})$, the direct normal irradiance (DNI), and the geometrical concentration ratio was assumed to be 85%, 1000 W/m^2 and between 100-1000 sun, respectively.

3.1 Boundary Conditions

Azur Space 3C44- 3×3 mm^2 cell area was modelled as one block of germanium (Ge), as considered by other authors[4,20,24,47,49]. The thermal boundary conditions applied to the system can be seen in Figure 6. Substrates and fin heat-sink, as a consecutive component for the solar cell in building-up the CPV system, was modelled using material of different layers and thicknesses (Figure 5) and using the thermo-physics properties of each layer table 1. Density and thermal conductivity had been set to be independent, no variation with temperature. Solder material was considered as thin thermal resistive layers. All the analyzed inputs and boundary conditions in the simulations are summarized in table 2 and Figure 6.

Table 2 Input parameters for the simulations and thermal boundary conditions for Figure 6

Components	*Symbols*	Value	Units
Solar Cell	A_c	3 × 3	mm^2
	DNI	1000	W/m^2
	η *electric*	42.5	%
	η *optical*	85	%
	Concentration ratio	100 - 1000	Sun
Substrates	*Area*	3 × 3	mm^2
	Type	Direct Bonded Copper (DBC)	
		Insulated Metal Substrates (IMS)	
		Silicon Wafer (Si Wafer)	
Fin heat-sink	*Baseplate thickness*	0.8	μm^2
	Baseplate Width	5	cm
	Baseplate Length	5	cm
	Materials	Aluminium	
		Copper	
		Silicon	
CPV system	*h*	3 - 25	$W/ m^2. K$
	T_a	20 – 56	℃

Thermal Boundary conditions		
Number	**Region**	**Boundary Condition**
1	*Solar Cell*	*Boundary heat Source*
2	*All free surfaces and micro-fin heat-sin*	*Natural Convection*
3		
4	*All Side surfaces of the heat-sink baseplate*	*Adiabatic* $q = 0$
5	*Surrounding*	*Ambient Temperature*

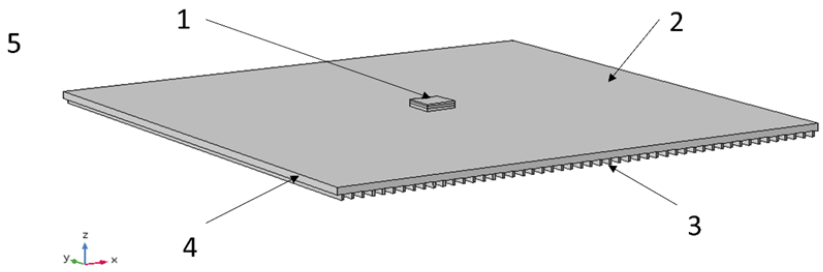

Figure 6 Thermal Boundary Condition

3.2 Meshing

Meshing is a key process when using the finite element method. The accuracy and the time it takes to solve the model is strongly related to the mesh set-up. In this study, different sizes of meshing were applied to ensure the optimal meshing size in every domain. The thickness of the thin layers in the substrates was smaller than the smallest element size for the predefined value in extremely fine mesh in COMSOL. The tetrahedral mesh was introduced to customize the maximum and the minimum element size to be within the thickness of the thin layer by taking into consideration the required computational time, as in Figure 7.

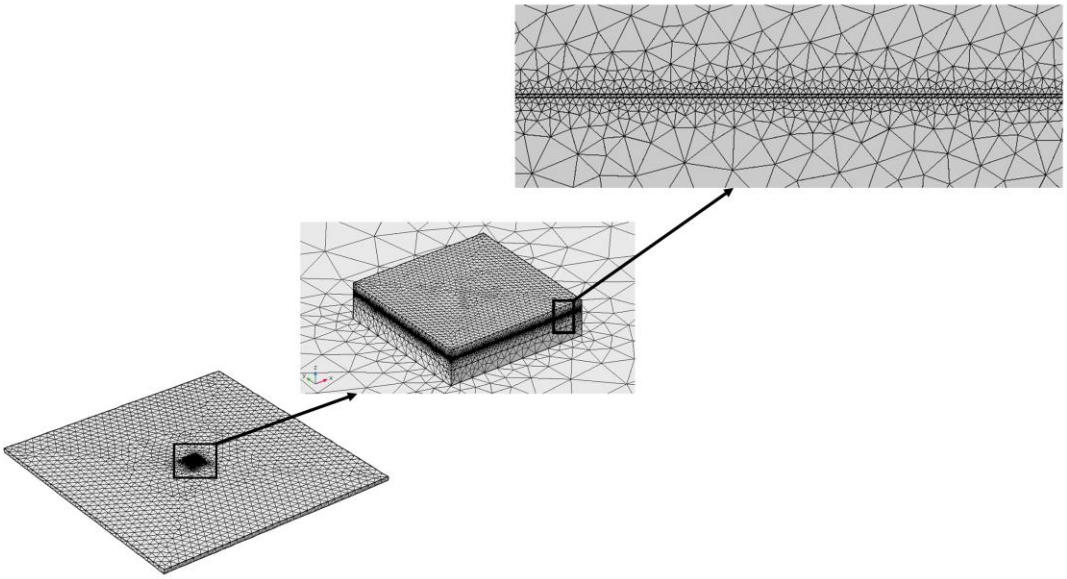

Figure 7 Tetrahedral mesh applied to the thin layer.

Different mesh sizes were simulated at 1000 × concentration ratio. The cell temperature obtained at every mesh size is used to consider the relative error between consecutive mesh sizes and to consider the computational time. The maximum cell temperature was simulated to be 156.39 °C and 156.47 °C for mesh size ranged from extremely coarser to extremely fine

with a computational time from 4 s to 84 s, respectively. Thus, the normal mesh size was selected to give a temperature of 156.42 °C. The normal mesh size results in a relative error of 0.03% to the asymptotic value at extremely fine meshing, as in Figure 8.

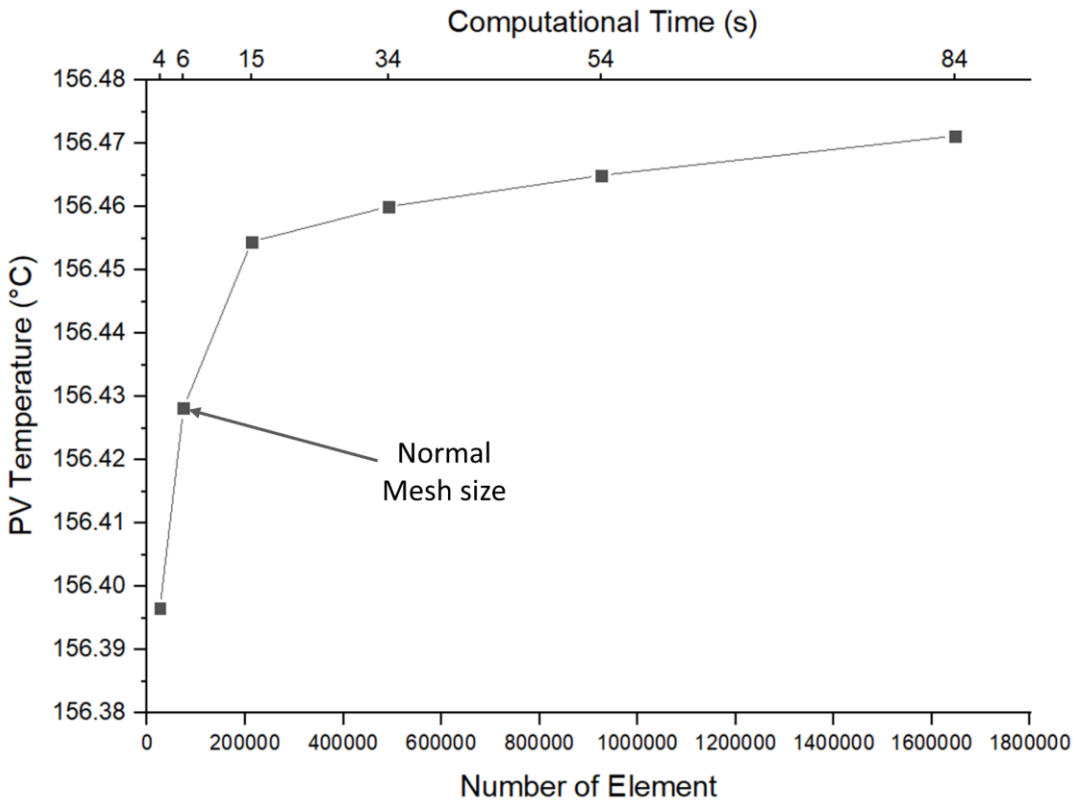

Figure 8 Mesh selection study for cell temperature (micro-finned heat-sink with DBC substrate at 1000 suns).

4. Results

In this work, the HCPV was subjected to operate in the worst-case conditions (WCCs) wherein the cell is not capable of producing any electrical power ($\eta_{electrical} = 0$). Thus, all the sunlight incident on the solar cell is to be dissipated as heat. In this condition, the cell temperature rapidly elevates rapidly. For safe operation, the solar cell must not exceed 110 °C, which is the maximum operating temperature of 3C44C Azur Space.

We validated the model by comparison with previous studies for the same solar cell size and heatsink configuration. First, we adjusted the developed thermal model to the same conditions in [18] with no heatsink to predicted the cell temperature under a concentration ratio in the range of 100 -1000 Suns, and the results of the current study are in good agreement with [18,26] with an average error factor of 2.7 %, as in Figure 9.

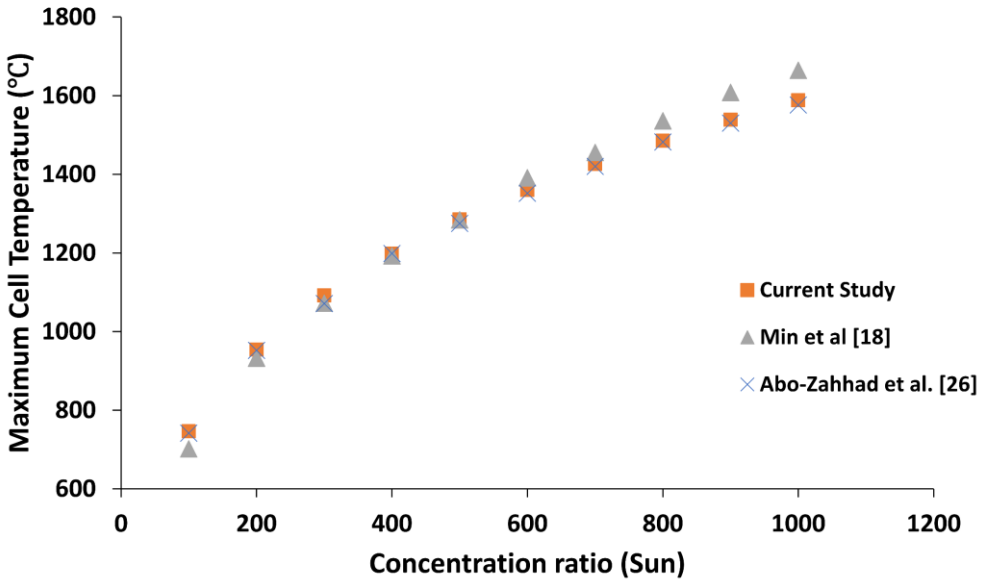

Figure 9 Validation for the predicted maximum cell temperature with Min et al. [18] and Abo-Zahhad et al. [26] with no cooling aid for DBC substrates

Second, the thermal model was adjusted for standard operating test conditions (SOTC) allowing the cell to produce electrical power ($\eta_{electrical} = 42.5\%$) at 500 suns for a flat-plate heatsink. Table 3 shows a significant agreement between this study and [5,50].

Table 3 Validation with the previous study

	DBC [°C]	IMS [°C]	Si wafer [°C]
Current Study	75.11	71.2	77
Micheli et al [5]	75	72.8	78.8
Current Study	74	-	-
Algora et al [50]	73	-	-

4.1 Performance characteristics of CPV with flat-Plate and micro-fin heat sinks

Utilizing the COMSOL Multiphysics numerical simulation model, we can predict the maximum cell temperature for a 3x3 mm^2 solar cell mounted on DBC, IMS, and Si wafer attached with a flat-plate and micro-finned heat-sink under concentration ratios ranging from 100 to 1000 suns. Copper, aluminum, and silicon were selected as the heat-sink materials for DBC, IMS, and Si wafer, respectively. Figure 10 shows the temperature contours of the solar cell when using different substrate materials and using micro fin heat sinks.

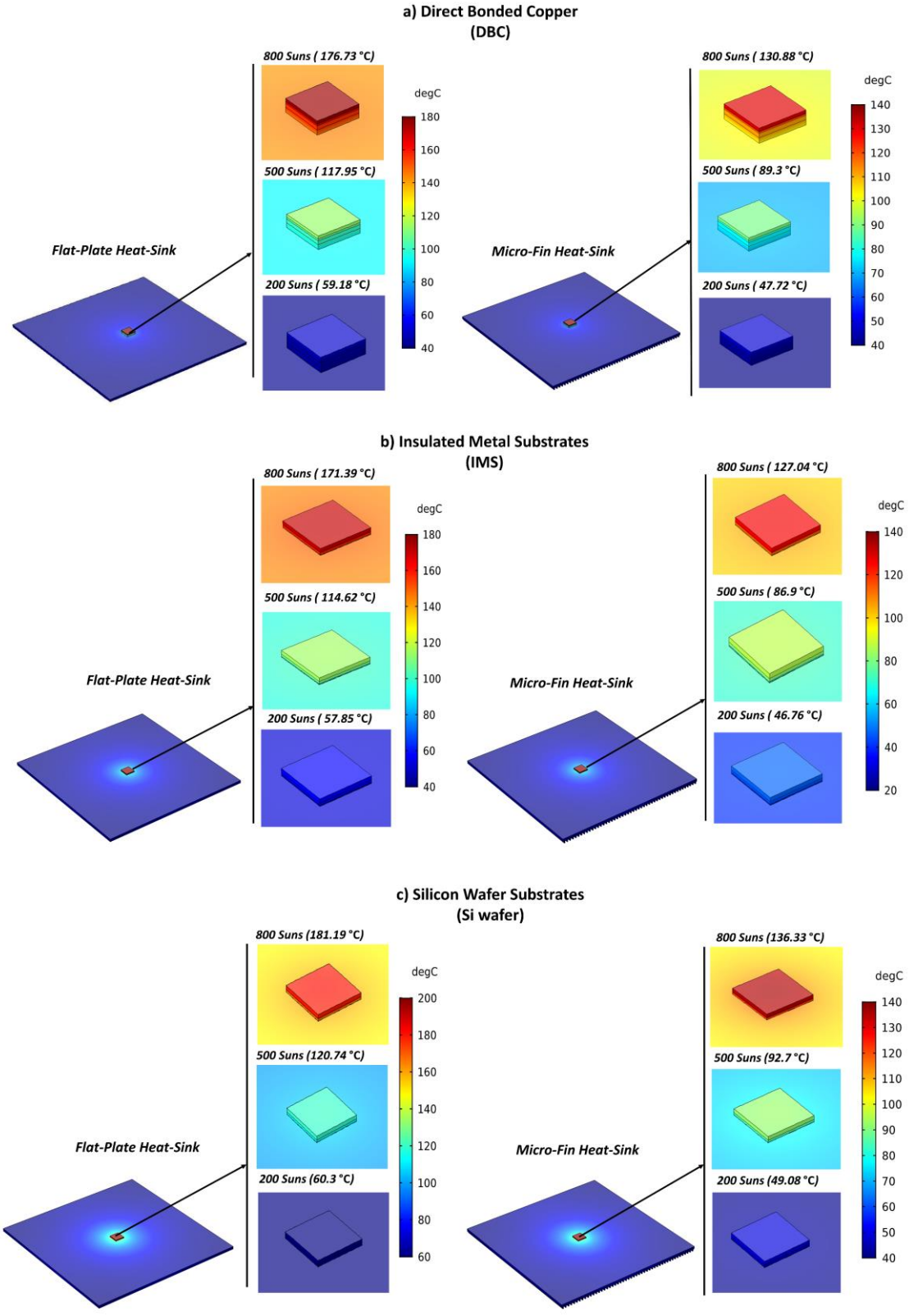

Figure 10 Temperature field distribution for a) Direct Bonded Copper (DBC), b) Insulated Metal Substrates (IMS), and c) Silicon Wafer Substrate (Si Wafer)

Even as the concentration ratio increased, the cell on the micro-finned heat-sink exhibited a lower maximum cell temperature compared to the system with a flat-plate heat-sink. The difference in maximum temperature between the flat-plate heat-sink and micro-finned heat-sink increased linearly. As shown in Figure 11, the switching values from passive to active cooling for the flat plate is 305.7, 316.6 and 296.2 suns for DBC, IMS, and Si wafer; whereas, the switching value for micro-finned are 433.7, 450 and 411.8 suns for DBC, IMS, and Si wafer, respectively. The introduction of the micro-finned heat sink results in 25.32%, 23.13%, and 22.24% as an average drop in temperature for DBC, IMS, and Si wafer, respectively. The result shows an average increase of 0.254 °C, 0.248 °C, and 0.26 °C for every Sun in the flat-plate heat-sinks for DBC, IMS, and Si wafer; whereas, the result shows an average increase of 0.197 °C, 0.192 °C, and 0.204°C for every Sun in the micro-finned heat-sinks for DBC, IMS, and Si wafer, respectively. At 1000 suns the micro-finned heat sink showed a much lower temperature than the flat-plate heat sinks. It can be seen in Figure 11 that this was 57.31 °C, 55.43 °C, and 56.07 °C for the micro-finned DBC, IMS, and Si wafer heat sinks respectively.

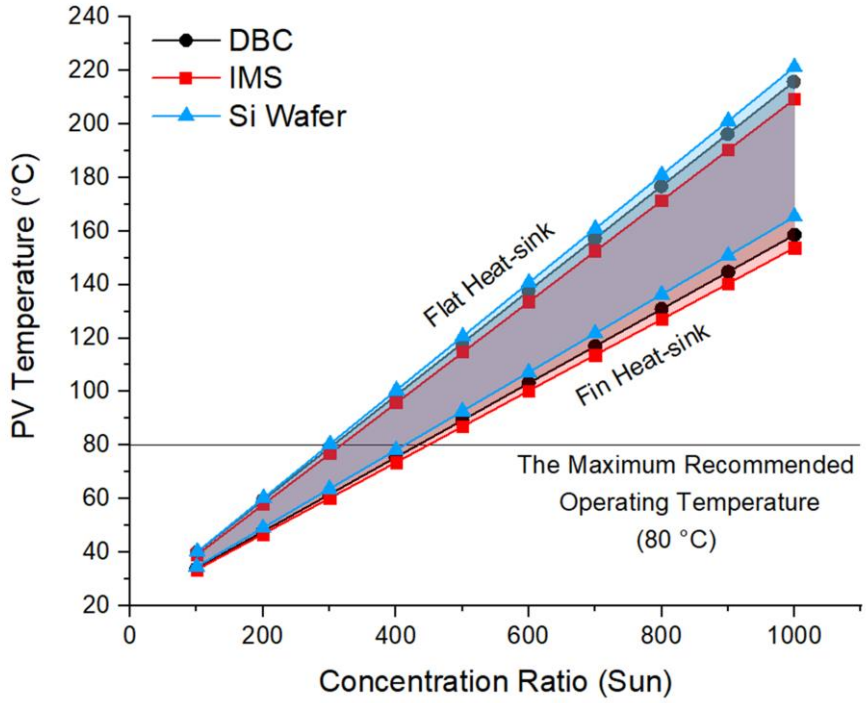

Figure 11 Simulated maximum temperature for the solar cell mounted on DBC, IMS, and Si wafer.

4.2 Impact of increasing convective heat transfer coefficient

The convective heat transfer is classified according to the nature of the flow and is dependent on the wind speed and the temperature gradient. Forced convection is caused by

external intervention. However, for natural convection, the temperature gradient induces the density differences causing a buoyancy force within the air to move. The CPV system is subjected to external winds which impacts the operating solar cell temperature.

The impact of the wind speed is studied by varying the convective heat transfer coefficient in the natural convection range of $3 - 25\left[\frac{W}{m^2.K}\right]$ in an interval of $2\left[\frac{W}{m^2.K}\right]$ at an ambient temperature of 20 °C for the micro-fin heat-sink. The results showed that the cell temperature is linearly dependent on the concentration ratio, as shown in Figure 12.a. Also, the cell temperature dependency on the convective heat transfer has a strong effect up to $14\left[\frac{W}{m^2.K}\right]$and then the drop-in cell temperature begins diminishing. Clearly, the higher the convective heat transfer coefficient, the lower the cell temperature meaning high exploitation of natural air circulation. The solar cell on the DBC substrate was found to have a maximum temperature of 429.38°C at 1000 suns under the lowest convective heat transfer coefficient of $4\left[\frac{W}{m^2.K}\right]$ and goes down to 129.57°C using a convective heat transfer coefficient of $22\left[\frac{W}{m^2.K}\right]$. The solar concentration limits for safe operation also increase with the increasing heat transfer coefficient. As shown in Figure 12.a. the solar concentration limits increase by 401.3 suns, 507.5 suns, and 431.2 suns for the DBC, IMS, and Si wafer, respectively.

Using linear interpolation, we identified the concentration ratio limits for a range of convective heat transfer coefficient whilst maintaining an 80 °C maximum recommended operating temperature. The concentration ratio limits are plotted for DBC, IMS and Si wafer in Figure 12.b.

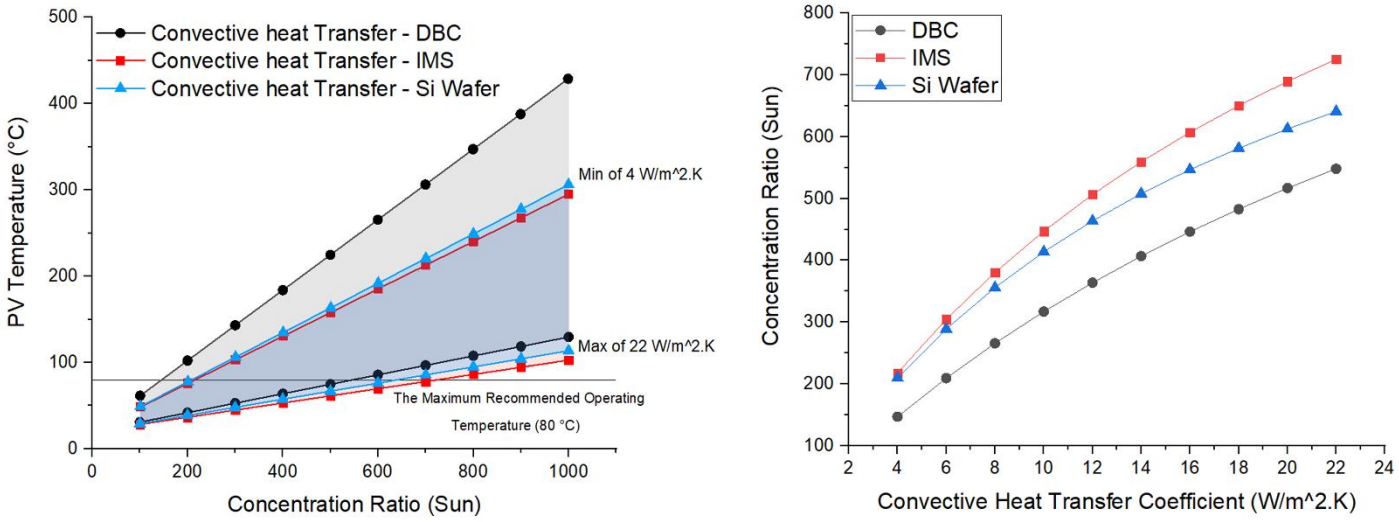

Figure 12 a. cell temperature with concentration ratio and convective heat transfer coefficient range for DBC, IMS, and Si wafer and b. Concentration ratio limits with convective heat transfer coefficient for DBC, IMS, Si wafer.

4.3 Impact of ambient temperature and increasing Concentration ratio

One of the important parameters that influence the PV performance is the ambient temperature. In the present study, we vary the ambient temperature taking it from a nominal value of 20°C to extreme weather condition of 56 °C. The selection of the temperature range is made to accommodate the historical day temperatures in countries like Saudi Arabia, India and Spain where these CPV systems would be typically deployed.

Studies were carried out to evaluate the performance of the micro-fin heat-sink varying the ambient temperature, concentration ranges 100 – 1000 suns and at a fixed convective heat transfer coefficient 10 W/m^2. K. The incremental linear correlations between the cell temperature and ambient temperature are shown in Figure 13.a. It was observed that for every degree increment of the ambient temperature between 100-1000 sun, the cell temperature for DBC, IMS, and Si wafer increased by 123.08 °C, 120.72 °C, and 130.87 °C, respectively. Obviously, a lower ambient temperature results in better heat exchange with the surrounding reducing by that the cell temperature and allowing the cell to accept a higher concentration ratio. Increasing the ambient temperature from 20 – 56 °C reduces the concentration ratio limits by 265.4 suns, 267.2 suns, and 249.6 suns for the DBC, IMS, Si wafer, respectively. The results obtained were extrapolated to determine the concentration ratio limits with ambient temperature at 80 °C and plotted for DBC, IMS and Si wafer as in Figure 13.b.

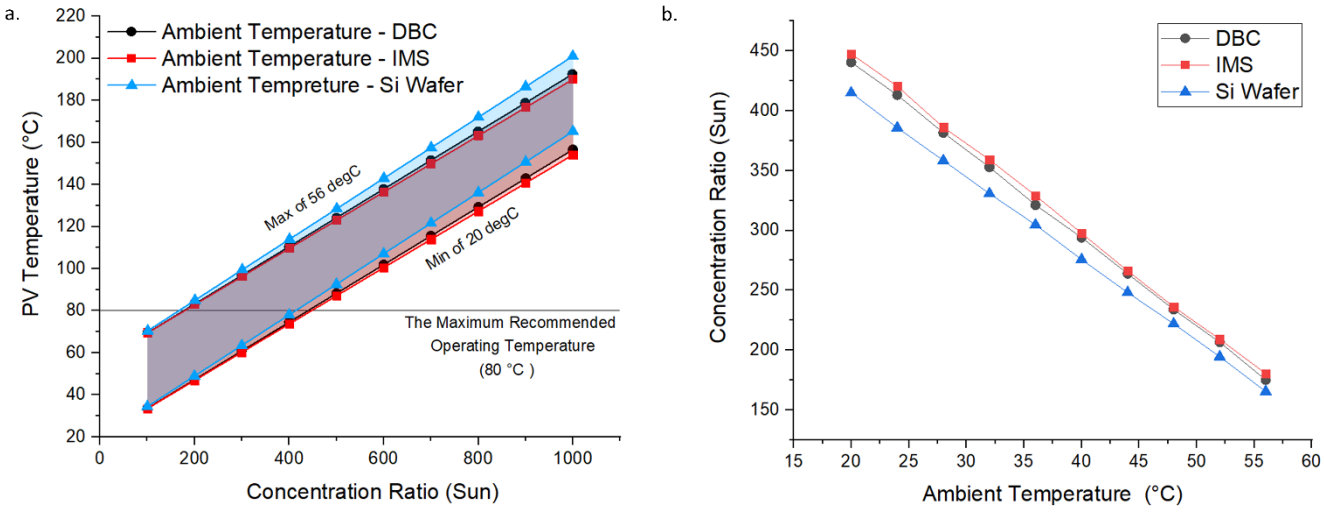

Figure 13 a. PV temperature with concentration ratio at a range of ambient temperature value for DBC, IMS, and Si wafer and b. concentration ratio limits with ambient temperature for DBC, IMS, and Si wafer

It can be seen clearly that the solar concentration needs to decrease for optimal operation at places with higher ambient temperatures. The most comfortable range to operate under any of these extreme conditions would be in the range of 100-200suns.

4.4 Impact of varying the number of micro-fins

Fins can play a crucial role in dissipating the heat from the substrate. Different types of fins with different shapes and sizes can be utilized. However, in our study we have used micro fins with a linear profile and varied them between 10 – 120 maintaining a fixed fin thickness. It is important to note that increasing the micro-fin number also reduces the pitch spacing between them. The thermal model was performed based on convective heat transfer at 10 W/ m^2. K and ambient temperature at 20 °C assuming, there is no effect by the reduction in the spacing between micro-fin. To configure the micro-fin on the baseplate for spacing evenly, the following equations (9) were conducted in the thermal model

$$X_1 = \frac{\frac{Baseplate\ Width}{2}}{Micro{-}fin\ number} \qquad \text{position of first micro-fin}$$

$$X_2 = X_1 + \frac{Baseplate\ Width}{micro{-}fin\ number} \qquad \text{position of second micro-fin}$$

$$X_n = X_1 + X_2 + X_n + \frac{Baseplate\ Width}{micro{-}fin\ number} \qquad \text{position of consecutive micro-fins} \qquad (9)$$

Where X is the position of micro-fin localized along the baseplate width and distributed based on the micro-fin number. As in Figure 14.a. the results show a linear dependency of cell temperature on the concentration ratio. The maximum safe operating concentration ratio range increases to up to 600 suns when using a micro finned heat sink of up to 120 fins. Increasing the number of fins helps improve the heat dissipation from the heat sink. It was found that increasing the number of fins from 20 – 120 fins results in improving the concentration ratio limits by 233.7 suns, 250 suns, and 216.9 suns for the DBC, IMS, and Si wafer, respectively.

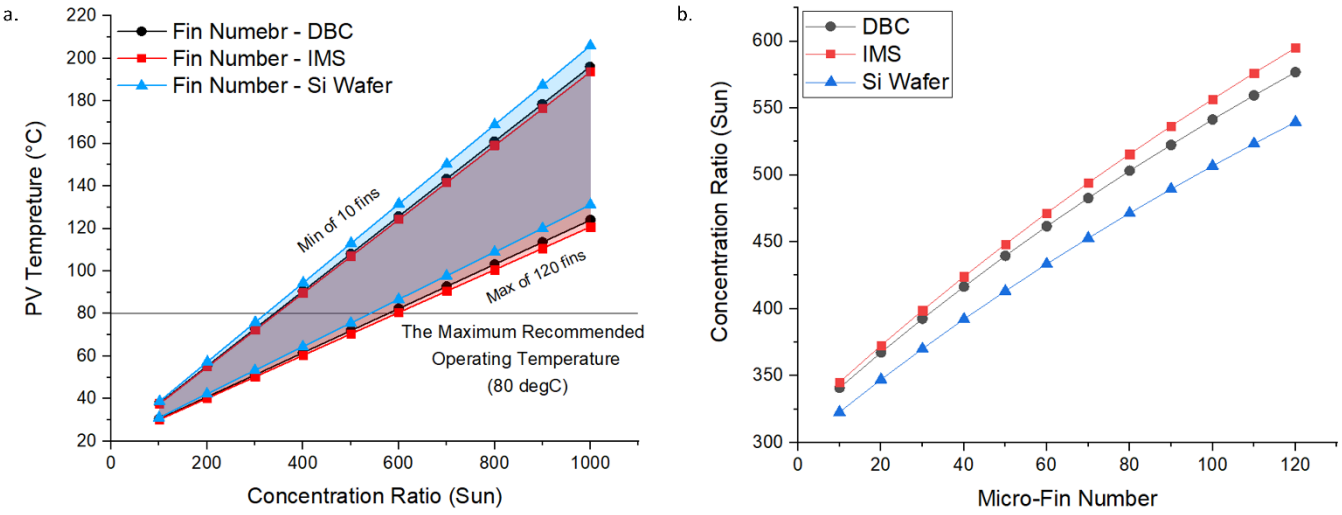

Figure 14 a. PV temperature with concentration ratio at a range of micro-fin number for DBC, IMS, and Si wafer and b. Concentration ratio limits with micro-fin number for DBC, IMS and Si wafer

The manufacturing techniques of micro-fins out of metals are laborious process at which the cost of machining a micro scaling fin is primarily related to the machining time. Thus, the limits of concentration ratio at 80 °C for a large number of fins clearly increases but at the price of required machining time as shown in Figure 4 and Figure 14.b.

Table 4 The concentration ratio limits with a range of micro-fin number.

Micro-Fin Number	Concentration ratio at 80 °C (Sun)		
	DBC	**IMS**	**Si Wafer**
10	340.8	345.1	322.7
20	367.3	372.6	347.1
30	392.5	398.8	370.1
40	416.5	424.1	392.2
50	439.6	448.3	413.2
60	461.7	471.6	433.5
70	482.7	494.1	452.8
80	503.2	515.7	471.5
90	522.5	536.6	489.5
100	541.5	556.7	506.8
110	559.5	576.3	523.5
120	576.9	595.1	539.6

5. Performance metrics and Outlook

CPV systems can be designed using a variety of heat sinks in order to dissipate heat and operate the solar cell at the desired operating temperature. If natural convection is the only available choice, then this would involve the use of sophisticated machining of the heat sinks in order to achieve the optimal operating conditions. Micro heat sinks have been widely used in a variety of applications including in space and the cooling of a variety of electronic equipment given their lightweight and small dimensions. In CPV applications the weight of the CPV module dictates the load for the tracker and hence makes it equally important to use lighter heat sinks.

The limitations posed by these heat sinks include their physical geometry, machining costs and the amount of heat that they can dissipate. In our study, we chose a standard design of a micro heat sink and evaluated its performance while changing its material properties, the number of fins and the operating variables. We studied a variety of substrate materials including DBC, Si wafer and IMS. The choice of the materials was based on previous research studies highlighting the advantages of different substrates. Silicon being a semiconductor has very similar thermal expansion properties to those of the solar cell and can help prevent

mechanical failure due to the mechanical stresses induced via thermal loading. DBC uses multiple layers of copper sheet enabling higher conduction of heat but has a higher thermal expansion coefficient. IMS is an alternative to DBC and has been very commonly used in the PCB industry making it the cheapest heat sink currently available.

The geometrical parameters of the heat sink dictate the performance limits of the CPV solar cell attached to them. The number of fins, the pitch and their shape can determine the amount of heat dissipation from these devices and ultimately enable the optimization of the system design. In our study, we maintained a linear fin geometry and heat sink area but varied the number of the fins and the pitch. Increasing the number of fins improved the heat dissipation rate but also increases the machining costs of the heat sink. The operating range of the CPV device also increased with an increase in the number of fins. We found that heat sinks using IMS at 10 W/m^2. K and an ambient temperature of 20°C were limited to its solar concentration of 595suns while using the maximum number of fins (120). Which leads us to the question of understanding the impact of the operating variables which can vary significantly in places with high DNI.

The key operating variables that influence the performance of the CPV system are the ambient temperature and the wind speed which determines the heat transfer coefficient available at the heat sinks. In our study, we have exhaustively varied the temperature range between 20-56°C and the heat transfer coefficient between 4-20 W/m^2. K. We found that both these parameters have a huge impact. For example, the maximum solar concentration of 595suns drastically decreases the IMS performance limit to 180 suns at 56 °C and 10 W/m^2. K. The increase in the heat transfer coefficient can have a positive impact becomes 22 W/m^2. K the performance limit of solar concentration increases to 725suns.

6. Conclusion

A 3D numerical model has been developed to predict the maximum cell temperature of micro-finned heat-sink in Fresnel based CPV under different concentration ratio levels for three different substrates materials using COMSOL. In the worst-case conditions, the developed model was able to determine the concentration ratio limits based on the solar cell maximum recommended temperature of 80 °C for different values of natural convective heat transfer coefficient, ambient temperature, and the number of fins. Based on the predicted results, we reached the following:

1- Micro-finned heat sink showed 57.31 °C, 55.43 °C, and 56.07 °C as a drop-in temperature at 1000 suns in comparison with the flat-plate heatsink for the DBC, IMS, and Si wafer, respectively.
2- Increasing the convective heat transfer coefficient from 4 – 22 W/m^2. K allows the concentration limits to rise by 401.3 suns, 507.5 suns, and 431.2 suns for the DBC, IMS, and Si wafer, respectively.
3- Increasing the ambient temperature from 20 – 56 °C reduces the concentration ratio limits by 265.4 suns, 267.2 suns, and 249.6 suns for the DBC, IMS, Si wafer, respectively
4- Increasing the number of fins from 20 – 120 fins result in improving the concentration ratio limits by 233.7 suns, 250 suns, and 216.9 suns for the DBC, IMS, and Si wafer, respectively.

Clearly, the thermal resistance of Al2O3 in DBC, Marble resin in IMS, and Si3N4 in Si wafer generate a temperature gradient between the cell and the heat-sink material. However; the low thermal resistance of the IMS substrate results in the best thermal performance in terms of maintaining the cell temperature below 80 °C and allowing a wider range of high concentration ratio.

Acknowledgement

Mr Mussad Alzahrani would like to duly acknowledge the financial support from the Saudi Arabia Culture Bureau in the United Kingdom.

References

[1] Baig H, Heasman KC, Mallick TK. Non-uniform illumination in concentrating solar cells. Renewable and Sustainable Energy Reviews 2012;16:5890–909. https://doi.org/10.1016/j.rser.2012.06.020.

[2] Venkateswari R, Sreejith S. Factors influencing the efficiency of photovoltaic system. Renewable and Sustainable Energy Reviews 2019;101:376–94. https://doi.org/10.1016/j.rser.2018.11.012.

[3] Chan NLA, Ekins-Daukes NJ, Adams JGJ, Lumb MP, Gonzalez M, Jenkins PP, et al. Optimal bandgap combinations-does material quality matter. IEEE Journal of Photovoltaics 2012;2:202–8. https://doi.org/10.1109/JPHOTOV.2011.2180513.

[4] Valera A, Fernández EF, Rodrigo PM, Almonacid F. Feasibility of flat-plate heat-sinks using microscale solar cells up to 10,000 suns concentrations. Solar Energy 2019;181:361–71. https://doi.org/10.1016/j.solener.2019.02.013.

[5] Micheli L, Senthilarasu S, Reddy KS, Mallick TK. Applicability of silicon micro-finned

heat sinks for 500× concentrating photovoltaics systems. Journal of Materials Science 2015;50:5378–88. https://doi.org/10.1007/s10853-015-9065-2.

[6] Fernández EF, Almonacid F, Rodrigo P, Pérez-Higueras P. Calculation of the cell temperature of a high concentrator photovoltaic (HCPV) module: A study and comparison of different methods. Solar Energy Materials and Solar Cells 2014;121:144–51. https://doi.org/10.1016/j.solmat.2013.11.009.

[7] He YL, Wang K, Qiu Y, Du BC, Liang Q, Du S. Review of the solar flux distribution in concentrated solar power: Non-uniform features, challenges, and solutions. vol. 149. Elsevier Ltd; 2019. https://doi.org/10.1016/j.applthermaleng.2018.12.006.

[8] Wang Y, Liu Q, Lei J, Liu F. Design and characterization of the non-uniform solar flux distribution measurement system. Applied Thermal Engineering 2019;150:294–304. https://doi.org/10.1016/j.applthermaleng.2018.12.150.

[9] Araki K, Uozumi H, Yamaguchi M. A simple passive cooling structure and its heat analysis for 500× concentrator PV module 2003:1568–71. https://doi.org/10.1109/pvsc.2002.1190913.

[10] Segal A, Epstein M, Yogev A. Hybrid concentrated photovoltaic and thermal power conversion at different spectral bands. Solar Energy 2004;76:591–601. https://doi.org/10.1016/j.solener.2003.12.002.

[11] Vincenzi D, Baricordi S, Calabrese S, Musio M, Damiano A. A cassegrain concentrator photovoltaic system: Comparison between dichroic and multijunction photovoltaic configurations. IECON Proceedings (Industrial Electronics Conference) 2014:1900–5. https://doi.org/10.1109/IECON.2014.7048761.

[12] Kribus A, Kaftori D, Mittelman G, Hirshfeld A, Flitsanov Y, Dayan A. A miniature concentrating photovoltaic and thermal system. Energy Conversion and Management 2006;47:3582–90. https://doi.org/10.1016/j.enconman.2006.01.013.

[13] Helmers H, Boos A, Jetter F, Heimsath A, Wiesenfarth M, Bett AW. Outdoor test setup for concentrating photovoltaic and thermal (CPVT) systems. AIP Conference Proceedings 2011;1407:175–9. https://doi.org/10.1063/1.3658320.

[14] Otanicar TP, Taylor RA, Telang C. Photovoltaic/thermal system performance utilizing thin film and nanoparticle dispersion based optical filters. Journal of Renewable and Sustainable Energy 2013;5. https://doi.org/10.1063/1.4811095.

[15] Jakhar S, Soni MS, Gakkhar N. Historical and recent development of concentrating photovoltaic cooling technologies. Renewable and Sustainable Energy Reviews 2016;60:41–59. https://doi.org/10.1016/j.rser.2016.01.083.

[16] Royne A, Dey CJ, Mills DR. Cooling of photovoltaic cells under concentrated illumination: A critical review. Solar Energy Materials and Solar Cells 2005;86:451–83. https://doi.org/10.1016/j.solmat.2004.09.003.

[17] Micheli L, Sarmah N, Luo X, Reddy KS, Mallick TK. Opportunities and challenges in micro- and nano-technologies for concentrating photovoltaic cooling : A review. Renewable and Sustainable Energy Reviews 2013;20:595–610. https://doi.org/10.1016/j.rser.2012.11.051.

[18] Cui M, Chen N, Yang X, Wang Y, Bai Y, Zhang X. Thermal analysis and test for single concentrator solar cells. Journal of Semiconductors 2009;30. https://doi.org/10.1088/1674-4926/30/4/044011.

[19] Gualdi F, Arenas O, Vossier A, Dollet A, Aimez V, Arès R. Determining passive cooling limits in CPV using an analytical thermal model. AIP Conference Proceedings 2013;1556:10–3. https://doi.org/10.1063/1.4822187.

[20] Chow S, Valdivia CE, Wheeldon JF, Ares R, Arenas OJ, Aimez V, et al. Thermal test and simulation of alumina receiver with high efficiency multi-junction solar cell for concentrator systems. Photonics North 2010 2010;7750:775035. https://doi.org/10.1117/12.872894.

[21] Wang Y, Liu Q, Lei J, Liu F. Design and characterization of the non-uniform solar flux distribution measurement system. Applied Thermal Engineering 2019;150:294–304. https://doi.org/10.1016/j.applthermaleng.2018.12.150.

[22] Renzi M, Egidi L, Comodi G. Performance analysis of two 3.5 kWp CPV systems under real operating conditions. Applied Energy 2015;160:687–96. https://doi.org/10.1016/j.apenergy.2015.08.096.

[23] Chou TL, Shih ZH, Hong HF, Han CN, Chiang KN. Thermal performance assessment and validation of high-concentration photovoltaic solar cell module. IEEE Transactions on Components, Packaging and Manufacturing Technology 2012;2:578–86. https://doi.org/10.1109/TCPMT.2011.2181165.

[24] Theristis M, O'Donovan TS. Electrical-thermal analysis of III-V triple-junction solar cells under variable spectra and ambient temperatures. Solar Energy 2015;118:533–46. https://doi.org/10.1016/j.solener.2015.06.003.

[25] Micheli L, Reddy KS, Mallick TK. Plate micro-fins in natural convection: An opportunity for passive concentrating photovoltaic cooling. Energy Procedia 2015;82:301–8. https://doi.org/10.1016/j.egypro.2015.12.037.

[26] Abo-Zahhad EM, Ookawara S, Radwan A, El-Shazly AH, El-Kady MF, Esmail MFC. Performance, limits, and thermal stress analysis of high concentrator multijunction solar cell under passive cooling conditions. Applied Thermal Engineering 2020;164:114497. https://doi.org/10.1016/j.applthermaleng.2019.114497.

[27] Hu H, Yuan D, Wang T, Jiang Y. Dynamic performance of high concentration photovoltaic/thermal system with air temperature and humidity regulation system (HCPVTH). Applied Thermal Engineering 2019;146:577–87. https://doi.org/10.1016/j.applthermaleng.2018.10.028.

[28] Abo-Zahhad EM, Ookawara S, Radwan A, El-Shazly AH, Elkady MF. Numerical analyses of hybrid jet impingement/microchannel cooling device for thermal management of high concentrator triple-junction solar cell. Applied Energy 2019;253:113538. https://doi.org/10.1016/j.apenergy.2019.113538.

[29] Maka AOM, O'Donovan TS. Modelling of the thermal behaviour of solar high concentrating photovoltaic receiver. Thermal Science and Engineering Progress 2019;9:281–8. https://doi.org/10.1016/j.tsep.2018.12.001.

[30] Aldossary A, Mahmoud S, Al-dadah R. Technical feasibility study of passive and active cooling for concentrator PV in harsh environment. Applied Thermal Engineering 2016;100:490–500. https://doi.org/10.1016/j.applthermaleng.2016.02.023.

[31] Wang S, Shi J, Chen HH, Schafer SR, Munir M, Stecker G, et al. Cooling design and evaluation for photovoltaic cells within constrained space in a CPV/CSP hybrid solar system. Applied Thermal Engineering 2017;110:369–81. https://doi.org/10.1016/j.applthermaleng.2016.08.196.

[32] Natarajan SK, Mallick TK, Katz M, Weingaertner S. Numerical investigations of solar cell temperature for photovoltaic concentrator system with and without passive cooling arrangements. International Journal of Thermal Sciences 2011;50:2514–21. https://doi.org/10.1016/j.ijthermalsci.2011.06.014.

[33] Sendhil Kumar N, Matty K, Rita E, Simon W, Ortrun A, Alex C, et al. Experimental validation of a heat transfer model for concentrating photovoltaic system. Applied Thermal Engineering 2012;33–34:175–82. https://doi.org/10.1016/j.applthermaleng.2011.09.031.

[34] Do KH, Kim TH, Han YS, Choi B Il, Kim MB. General correlation of a natural convective heat sink with plate-fins for high concentrating photovoltaic module cooling. Solar Energy 2012;86:2725–34. https://doi.org/10.1016/j.solener.2012.06.010.

[35] Mittelman G, Dayan A, Dado-Turjeman K, Ullmann A. Laminar free convection underneath a downward facing inclined hot fin array. International Journal of Heat and Mass Transfer 2007;50:2582–9. https://doi.org/10.1016/j.ijheatmasstransfer.2006.11.033.

[36] Bar-Cohen A, Iyengar M, Kraus AD. Design of Optimum Plate-Fin Natural Convective Heat Sinks. Journal of Electronic Packaging 2003;125:208. https://doi.org/10.1115/1.1568361.

[37] Kim JS, Park BK, Lee JS. Natural convection heat transfer around microfin arrays. Experimental Heat Transfer 2008;21:55–72. https://doi.org/10.1080/08916150701647835.

[38] Micheli L, Reddy K, Mallick TK. Plate Micro-Fins in Natural Convection: Experimental Study on Thermal Effectiveness and Mass Usage. International Conference on Polyaeneration 2013. https://doi.org/00.0000/PhysRevLett.000.000000.

[39] Micheli L, Reddy KS, Mallick TK. General correlations among geometry, orientation and thermal performance of natural convective micro-finned heat sinks. International Journal of Heat and Mass Transfer 2015;91:711–24. https://doi.org/10.1016/j.ijheatmasstransfer.2015.08.015.

[40] Mahmoud S, Al-Dadah R, Aspinwall DK, Soo SL, Hemida H. Effect of micro fin geometry on natural convection heat transfer of horizontal microstructures. Applied Thermal Engineering 2011;31:627–33. https://doi.org/10.1016/j.applthermaleng.2010.09.017.

[41] Luo Q, Li P, Cai L, Chen X, Yan H, Zhu H, et al. Experimental investigation on the heat dissipation performance of fl ared- fi n heat sinks for concentration photovoltaic

modules. Applied Thermal Engineering 2019;157:113666. https://doi.org/10.1016/j.applthermaleng.2019.04.076.

[42] Incropera F., Bergman T., Lavine A., DeWitt D. Fundamentals of heat and mass transfer. Wiley; 2011.

[43] Data M, Average T, Data E. Concentrator Triple Junction Solar Cell Cell Type : 3C44C- 3 × 3 mm2 Azur Space 2012:3–6.

[44] Micheli L, Sarmah N, Fernandez EF, Reddy KS, Mallick TK. Technical issues and challenges in the fabrication of a 144-Cell 500× Concentrating Photovoltaic receiver. 2014 IEEE 40th Photovoltaic Specialist Conference, PVSC 2014 2014:2921–5. https://doi.org/10.1109/PVSC.2014.6925543.

[45] Concentrator MJ, Assembly C. *Prototype Product. Area 2010;91342.

[46] Azur Space Solar Power GMBH. Enhanced Fresnel Assembly - EFA Type: 3C42A – with 10x10mm^2 CPV TJ Solar Cell Application: Concentrating Photovoltaic (CPV) Modules 2014:0–4.

[47] Micheli L, Sarmah N, Luo X, Reddy KS, Mallick TK. Design of a 16-cell densely-packed receiver for high concentrating photovoltaic applications. Energy Procedia 2014;54:185–98. https://doi.org/10.1016/j.egypro.2014.07.262.

[48] Mabille L, Mangeant C, Baudrit M. Development of CPV solar receiver based on insulated metal substrate (IMS): Comparison with receiver based on the direct bonded copper substrate (DBC) - A reliability study. AIP Conference Proceedings 2012;1477:289–93. https://doi.org/10.1063/1.4753888.

[49] Peharz G, Ferrer Rodríguez JP, Siefer G, Bett AW. A method for using CPV modules as temperature sensors and its application to rating procedures. Solar Energy Materials and Solar Cells 2011;95:2734–44. https://doi.org/10.1016/j.solmat.2011.03.030.

[50] Algora, Carlos Rey-Stolle I. Algora, Carlos Rey-Stolle, Ignacio. (2016). Handbook of Concentrator Photovoltaic Technology - 5.3.3.2 Solar Cell Packaging for Efficient Heat Transfer. John Wiley & Sons; 2016.